Check for updates

Geophysical Research Letters

RESEARCH LETTER
10.1029/2022GL098607

Future Amplification of Sea Surface Temperature Seasonality Due To Enhanced Ocean Stratification

Anila Rani Jo[1,2], June-Yi Lee[1,2,3], Axel Timmermann[1,4], Fei-Fei Jin[5], Ryohei Yamaguchi[1,4], and Angeles Gallego[6]

[1]Center for Climate Physics, Institute for Basic Science, Busan, South Korea, [2]Department of Climate System, Pusan National University, Busan, South Korea, [3]Research Center for Climate Sciences, Pusan National University, Busan, South Korea, [4]Pusan National University, Busan, South Korea, [5]Department of Atmospheric Sciences, University of Hawaii at Manoa, Honolulu, HI, USA, [6]Department of Oceanography, University of Hawaii at Manoa, Honolulu, HI, USA

Abstract In many regions the projected future sea surface temperature (SST) response to greenhouse warming is larger in summer than in winter. What causes this amplification of the SST seasonal cycle has remained unclear. To determine robustness of the projected seasonal cycle intensification and ascertain underlying physical mechanisms we analyze a suite of historical and greenhouse warming simulations conducted with 13 coupled general circulation models in the Coupled Model Intercomparison Project Phase 5. In the Representative Concentration Pathway 8.5 scenario, the amplitude of SST seasonal cycle, defined as the difference between climatological maximum and minimum temperature, increases by 30% ± 20% on average by the end of 21st century. Analysis of a simplified mixed layer heat budget demonstrates that the amplification can be attributed to the increasing upper ocean stratification and hence shoaling of the annual-mean mixed layer. The projected intensification of SST seasonality may have important implications for future changes in marine ecosystems.

Plain Language Summary One of the robust projected climate changes in response to global warming is the amplification of seasonal cycle of sea surface temperature (SST) with larger warming occurring in summer than in winter, especially in the North Atlantic, North Pacific and South Indian Ocean. Here we investigate the underlying physical mechanisms using a suite of future greenhouse warming simulations. We show that for the high greenhouse gas emission scenario the amplitude of SST seasonality increases over the next 80 years by 30% ± 20% globally. Overall mean ocean warming increases the upper ocean stratification, which leads to a shoaling of the mixed layer. This implies that climatological air-sea heat fluxes impact a smaller ocean volume, which then leads to an increased SST response. Other heat budget terms play only a secondary role. The increased temperature seasonality could further impact plankton phenology and the climatology of upper ocean CO_2.

Key Points:

- Under the high greenhouse gas emission scenario, the seasonal amplitude of sea surface temperature (SST) is projected to increase by 30% ± 20% by the end of 21st century
- The intensification of SST seasonality is largely due to the shoaling of the annual mean mixed layer depth
- The advection term explains about 10%–40% of the change in SST seasonality depending on the region

Supporting Information:

Supporting Information may be found in the online version of this article.

Correspondence to:

A. R. Jo and J.-Y. Lee,
anilarani92@pusan.ac.kr;
juneyi@pusan.ac.kr

Citation:

Jo, A. R., Lee, J.-Y., Timmermann, A., Jin, F.-F., Yamaguchi, R., & Gallego, A. (2022). Future amplification of sea surface temperature seasonality due to enhanced ocean stratification. *Geophysical Research Letters*, *49*, e2022GL098607. https://doi.org/10.1029/2022GL098607

Received 9 MAR 2022
Accepted 20 APR 2022

Author Contributions:

Conceptualization: Anila Rani Jo, June-Yi Lee, Axel Timmermann, Fei-Fei Jin, Angeles Gallego
Methodology: Anila Rani Jo, June-Yi Lee, Axel Timmermann, Ryohei Yamaguchi
Supervision: June-Yi Lee, Axel Timmermann
Writing – original draft: Anila Rani Jo, June-Yi Lee, Axel Timmermann, Fei-Fei Jin, Ryohei Yamaguchi
Writing – review & editing: Anila Rani Jo, June-Yi Lee, Axel Timmermann

© 2022. The Authors.
This is an open access article under the terms of the Creative Commons Attribution-NonCommercial-NoDerivs License, which permits use and distribution in any medium, provided the original work is properly cited, the use is non-commercial and no modifications or adaptations are made.

1. Introduction

Sea surface temperature (SST) plays a crucial role in the interaction between the ocean and the atmosphere. SST patterns drive large scale wind-systems (Bjerknes, 1969), determine the global rainfall distribution (Deser et al., 2010; Schmitt, 2018) and influence marine ecosystems (Sunagawa et al., 2015; Thomas et al., 2012). It is therefore crucial to understand, how SST will respond to greenhouse warming in terms of its mean state and seasonal cycle. The amplitude of the climatological SST seasonal cycle is generally larger in the extratropical oceans than the tropical oceans and larger in the Northern Hemisphere (NH) than in the Southern Hemisphere (SH) (Figure 1a). The seasonal cycle amplitude of SST is defined as the difference between annual maximum and minimum temperature (see Figure S1 in Supporting Information S1).

According to recent observational analyses, annual-mean global SST has increased by about 0.11 (0.09–0.13) °C per decade since 1970 (IPCC, 2019). Different versions of the Coupled Model Intercomparison Project demonstrated that this trend will continue in response to increasing greenhouse gas emissions (Alexander et al., 2018; Federation & Lynne, 2013; Gleckler et al., 2012). The projected multi-model mean change in global and annual mean SST by the end of the 21st century (2080–2100) relative to the recent past (1985–2005) attains values between 1.2°C and 3.0°C for Representative Concentration Pathway (RCP) 4.5 and 8.5 scenarios, respectively, based on 13 CMIP5 models (Taylor et al., 2012) (Figure 2a). CMIP5 models also simulate a robust decrease of

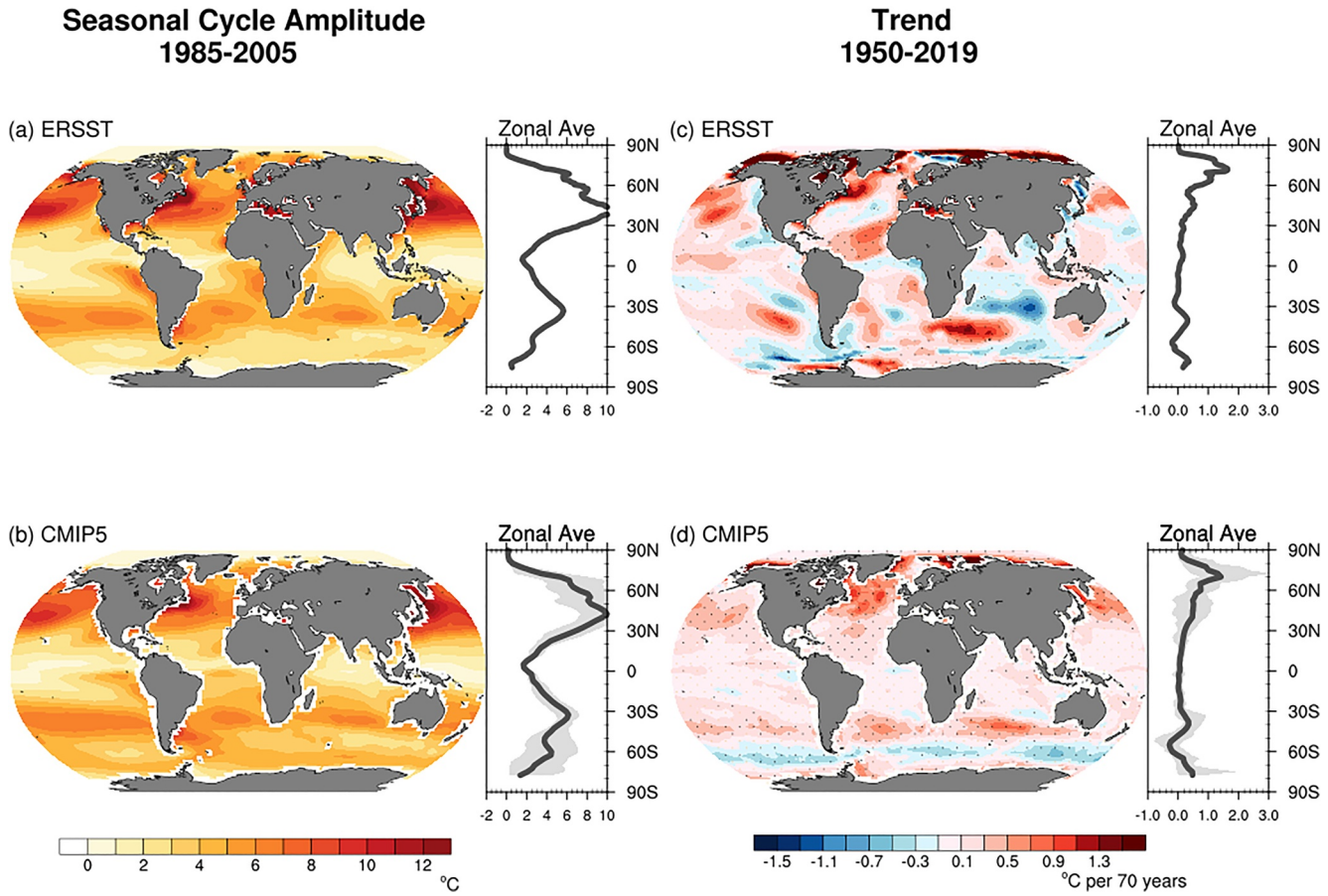

Figure 1. Climatological amplitude of sea surface temperature (SST) seasonal cycle for 1985–2005 (left panels) and its trend (right panels) from 1950 to 2019 for panel (a), (b) the observational (ERSSTv5) data (Huang et al., 2017) and panel (c), (d) the multi-model mean of 13 CMIP5 models, respectively. The seasonal cycle amplitude of SST is defined as the difference between annual maximum and minimum temperature. For models, historical simulations are used from 1950 to 2005 and Representative Concentration Pathway 8.5 runs from 2006 to 2019 to calculate the simulated trend. Black stippling in panels (c and d) indicates that the trend is statistically significant at 95% confidence level on the basis of *t*-test. ERSST stands for Extended Reconstruction of SST. Zonal average of each variable is also shown in the right side of map. For CMIP5, multi-model mean (thick solid line) and inter-model spread (gray shading-maximum to minimum) are shown.

the mixed layer depth (MLD) by about 10–15 m (Figure 2c). The CMIP6 models show similar results (Figure S2 in Supporting Information S1).

In addition to the increase in annual-mean SST, observational analyses show an increasing trend in the amplitude of the SST seasonal cycle for the last 70 years over many ocean basins (Figure 1b). The CMIP5 models realistically simulate not only its climatological distribution but also several characteristics of its trend patterns (Figures 1c and 1d). Consistent with the observed trend (Figure 1c) recent studies demonstrated a seasonal modulation of the projected SST trends, with stronger warming in summer than in winter (Alexander et al., 2018; Y. Y. Chen & Jin, 2018) (see Figure 1d).

It has been suggested that changes in the seasonal cycle of MLD may partly contribute to the stronger SST seasonality (Alexander et al., 2018). Gallego et al. (2018) showed that the SST seasonality is projected to amplify in most of the ocean basins in association with an increase in upper ocean stratification. Yamaguchi and Suga (2019) identified a pronounced strengthening of the ratio of summer-versus winter stratification in the mid- and high-latitude ocean in observational records. C. Chen & Wang (2015) presented amplification of SST annual cycle in the North Pacific responding to global warming attributable to the decrease of MLD in summer which will trap more incoming net heat flux and cause a higher SST increase than in winter. Other studies (e.g., Timmermann et al., 2004) suggested that projected changes in meridional SST gradients in the eastern equatorial Pacific can lead to an intensification of SST seasonality, with potential repercussions for ENSO (Karamperidou et al., 2020).

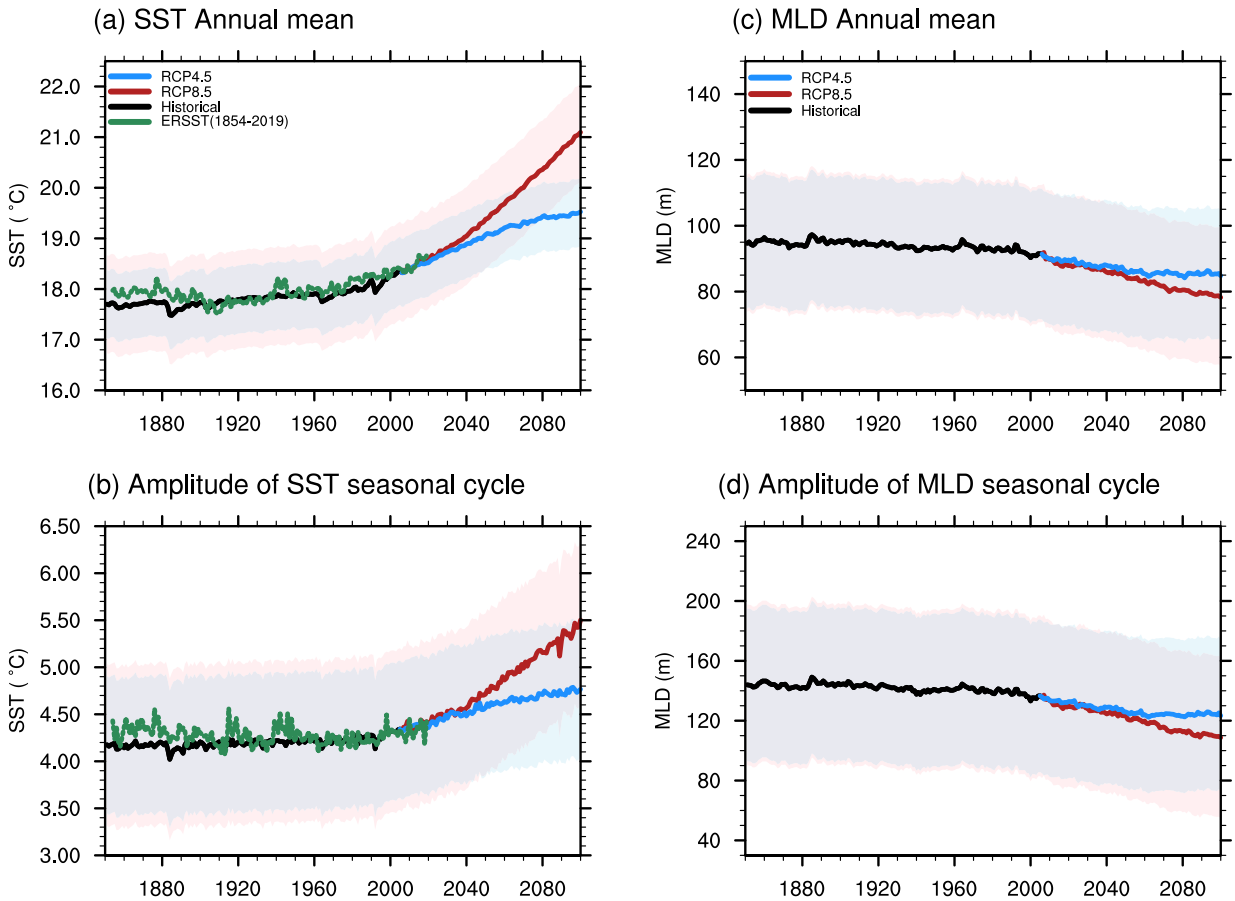

Figure 2. Multi-model mean (line) and inter-model spread (shading) for panel (a), (c) annual mean and panel (b), (d) seasonal cycle amplitude of spatial mean sea surface temperature (SST) (left panels) and spatial mean mixed layer depth (right panels) averaged over the globe, respectively, obtained from 13 CMIP5 models, respectively, during historical period (1851–2005) and the future (2006–2100). For the future projection, Representative Concentration Pathway (RCP) 4.5 and RCP 8.5 scenario in CMIP5 are used. The amplitude of seasonal cycle is calculated by subtracting the minimum value from the corresponding maximum value every year. Inter-model spread is obtained from one standard deviation against multi-model mean. The annual mean and seasonal cycle amplitude of SST based on ERSST from 1854 to 2019 are also shown in green in panels (a and b).

Recently, Liu et al. (2020) suggested that both the direct CO_2 and wind effect contribute to the enhancement of the SST seasonality based on single model experiments. In Liu et al. (2020), the contribution of the direct CO_2 effect in the absence of wind change was considered through the reduced wind mixing and warming-induced shoaling in the MLD under surface thermal forcing. However, the MLD contributions to the strengthening of SST seasonal cycle in their study were mostly inferenced statistically rather than qualitatively with a heat budget analysis.

While SST seasonality under present-day conditions is well understood, the mechanisms controlling the future seasonality are unclear. The aim of our study is to determine the mechanisms cause the intensification in the SST seasonal cycle and provide a better understanding of the spatial pattern of this amplification. In Section 2, models, data and methods used in this study are introduced. Section 3 addresses the main results on the amplification of SST seasonal cycle and its main drivers. The final section summarizes the major findings and discusses limitations of our approach which calls for further studies.

2. Methods

2.1. Models and Data

This study uses monthly mean SST and MLD, and calculates surface net heat flux using shortwave radiation, longwave radiation, latent heat flux and sensible heat flux from historical (1850–2005) and RCP 4.5 and 8.5 simulations (2006–2100) conducted as part of CMIP5 (Taylor et al., 2012). We focus our analysis on 13 out of 45 CMIP5

models. These models (Access1-0, CESM1-BGC, CanESM2, IPSL-CM5A-LR, Access1-3, CNRM-CM5, IPSL-CM5A-MR, IPSL-CM5B-MR, MPI-ESM-LR, MPI-ESM-LR, MRI-CGCM3, NorESM1-ME and NorESM1-M) were selected because their upper ocean mixed layer calculations include the effect of both temperature and salinity. We also evaluate two models (MPI-ESM1-2-HR and MPI-ESM1-2-LR) from CMIP6 (Eyring et al., 2016) which follow the Shared Socioeconomic Pathway2-4.5 and SSP5-8.5 scenario run (2015–2100). The analysis period covers the years 1985–2005 and 2080–2100. All data were regrided onto a common regular 2.5° × 2.5° longitude-latitude grid using Climate Data Operators (CDO) (Schulzweida, 2017).

We further used the Extended Reconstruction of SST version 5 (ERSSTv5) data (Huang et al., 2017) regrided onto 2.5° × 2.5° resolution to validate models. Figure 1 shows the long-term mean of the SST seasonal amplitude calculated for the recent past period (1985–2005) and its trend for 1950–2019 using the ERSSTv5 data set (upper panels) and 13 CMIP5 models (lower panels). The multi-model mean climatology of 13 CMIP5 models (Figure 1c) is in good agreement with the ERSSTv5 observations (Figure 1a).

2.2. SST Budget Analysis

To understand the underlying mechanisms driving amplification of the SST seasonal cycle, we performed a mixed layer heat budget analysis using the following simplified mixed layer temperature (T) equation:

$$\frac{dT}{dt} = \frac{Q}{\rho C_p h} - \left(u\frac{\partial T}{\partial x} + v\frac{\partial T}{\partial y} + w\frac{\partial T}{\partial z} \right) + \text{Res}, \tag{1}$$

with Q, ρ, C_p, h, u, v, w representing the net surface heat flux, density of sea water, specific heat capacity, MLD and zonal, meridional and vertical velocities respectively, and *Res* indicating the residual term including horizontal and vertical diffusion. Here, we assume that the contributions from the ocean advection terms and *Res* to the seasonal cycle of SST are small. This assumption is clearly not well justified in upwelling and boundary current regions, where strong velocities encounter large temperature gradients, but we shall see that several key aspects of the future amplification of the seasonal cycle can already be described from the heat flux and mixed layer terms. Thus, the mixed layer temperature equation considered here reads:

$$\frac{dT}{dt} \sim \frac{Q}{\rho C_p h}, \tag{2}$$

To determine the contributions to the SST seasonal cycle we first decompose each variable into two parts ($X(\text{month}) = \overline{X} + X'(\text{month})$). The term $\overline{X}$ represents the annual mean and X' denotes deviations from the annual mean (i.e., seasonal cycle in which interannual variability is seasonally interlocked). Thus, Equation 2 can be expressed in the following way.

$$\frac{d\left(\overline{T} + T'\right)}{dt} \sim \frac{\overline{Q} + Q'}{\rho C_p \left(\overline{h} + h'\right)} = \frac{\overline{Q} + Q'}{\rho C_p \overline{h}\left(1 + \frac{h'}{\overline{h}}\right)}. \tag{3}$$

Assuming $h' \ll \overline{h}$ (see Figure S3 in Supporting Information S1), the first order Taylor expansion of dT'/dt then reads

$$\frac{dT'}{dt} \approx \frac{Q'}{\rho C_p \overline{h}} - \frac{\overline{Q}\,h'}{\rho C_p \overline{h}^2} - \frac{Q'\,h'}{\rho C_p \overline{h}^2}. \tag{4}$$

The climatological monthly variation of SST can be determined by the seasonal cycle of the net surface heat flux (Q'), that of MLD (h') and product of Q' and h'. Equation 3 is the general form equation which we apply for the recent past (1985–2005) and the end of the 21st century (2080–2100). We use subscript 1 for the present and 2 for the future. Thus, the seasonal cycle of SST in the present and future can be written as

$$\frac{dT_1'}{dt} = \frac{Q_1'}{\rho C_p \overline{h_1}} - \frac{h_1'}{\rho C_p \overline{h_1}^2}\left(\overline{Q_1} - Q_1'\right), \tag{5}$$

$$\frac{dT_2'}{dt} = \frac{Q_2'}{\rho C_p \overline{h_2}} - \frac{h_2'}{\rho C_p \overline{h_2}^2}\left(\overline{Q_2} - Q_2'\right). \tag{6}$$

Then, the future seasonal cycle and annual mean can be written as $X_2{}' = X_1{}' + \delta X$ for the climatological seasonal cycle and $\overline{X}_2 = \overline{X}_1 + \Delta X$ for the climatological annual mean. Here, δX is the future change in seasonal cycle of X, and ΔX is the future change in climatological annual mean. The difference between Equations 5 and 6 represents the future change of the seasonal cycle of SST. Applying again a Taylor expansion to $\frac{1}{\left(1+\frac{\Delta h}{\overline{h}_1}\right)}$ and $\frac{1}{\left(1+\frac{\Delta h}{\overline{h}_1}\right)^2}$ ($\Delta h \ll \overline{h}_1$) (see Figure S4 in Supporting Information S1), the difference can be expressed as

$$\begin{aligned}\frac{d\delta T}{dt} = &\frac{\left(Q_1' + \delta Q\right)}{\rho C_p \overline{h_1}}\left(1 - \frac{\Delta h}{\overline{h}_1}\right) - \frac{\left(h_1' + \delta h\right)}{\rho C_p \overline{h_1}^2}\left(\overline{Q}_1 + \Delta Q\right)\left(1 - 2\frac{\Delta h}{\overline{h}_1}\right)\\ &+ \frac{\left(h_1' + \delta h\right)}{\rho C_p \overline{h_1}^2}\left(Q_1' + \delta Q\right)\left(1 - 2\frac{\Delta h}{\overline{h}_1}\right) - \frac{Q_1'}{\rho C_p \overline{h_1}} + \frac{h_1'}{\rho C_p \overline{h_1}^2}\left(\overline{Q_1} - Q_1'\right)\end{aligned} \tag{7}$$

For this budget analysis, the amplitude of seasonal cycle can be determined at every grid point by the difference between seasonal maximum and minimum. The month at which maximum and minimum local SSTs are attained can differ, depending on, local insolation, MLD and the seasonality of other feedback processes (Figure S1 in Supporting Information S1). Therefore, to properly evaluate this equation, we use temperature, heat fluxes and MLD that correspond to the season, when SST attains its minimum or maximum. For simplicity we assume that this peak occurrence does not change dramatically during the greenhouse warming simulation. Based on the SST seasonal cycle and based on the climatological monthly variation of SST (Equation 4 and Figure S1 in Supporting Information S1), we define the seasonal maximum (max) as the season in which SST peaks locally and seasonal minimum (min) as the season in which SST attains minimum value locally. The change in the amplitude of seasonal cycle of any variable X (δX_a) is calculated by δX (max)−δX (min) where max and min are determined for SST only and subscript a is used to define amplitude. Therefore, the change in the amplitude of SST seasonal cycle can be calculated as follows.

$$\begin{aligned}\frac{d\delta T_a'}{dt} = &-\frac{\left(h_1'\Delta Q\right)_a}{\rho C_p \overline{h_1}^2} + \frac{\delta Q_a}{\rho C_p \overline{h}_1} + \frac{\left(h_1'\delta Q\right)_a}{\rho C_p \overline{h_1}^2} - \frac{\left(Q_1'\Delta h\right)_a}{\rho C_p \overline{h_1}^2} + \frac{2\left(\overline{Q_1}\, h_1'\Delta h\right)_a}{\rho C_p \overline{h_1}^3} - \frac{2\left(Q_1' h_1'\Delta h\right)_a}{\rho C_p \overline{h_1}^3} - \frac{\left(\overline{Q_1}\,\delta h\right)_a}{\rho C_p \overline{h_1}^2}\\ &+ \frac{\left(Q_1'\delta h\right)_a}{\rho C_p \overline{h_1}^2} + \frac{2\left(h_1'\Delta Q\Delta h\right)_a}{\rho C_p \overline{h_1}^3} - \frac{(\Delta Q\delta h)_a}{\rho C_p \overline{h_1}^2} - \frac{(\delta Q\Delta h)_a}{\rho C_p \overline{h_1}^2} - \frac{2\left(h_1'\delta Q\Delta h\right)_a}{\rho C_p \overline{h_1}^3} + \frac{2\left(\overline{Q_1}\,\Delta h\delta h\right)_a}{\rho C_p \overline{h_1}^3}\\ &- \frac{2\left(Q_1'\Delta h\delta h\right)_a}{\rho C_p \overline{h_1}^3} + \frac{(\delta Q\delta h)_a}{\rho C_p \overline{h_1}^2} + \frac{2(\Delta Q\Delta h\delta h)_a}{\rho C_p \overline{h_1}^3} - \frac{2(\delta Q\Delta h\delta h)_a}{\rho C_p \overline{h_1}^3}\end{aligned} \tag{8}$$

3. Results

3.1. The Change in Amplitude of SST Seasonal Cycle

This section examines changes in the amplitude of SST seasonal cycle over the global ocean during the historical and future period based on 13 CMIP5 models. The timing of maximum and minimum SST varies spatially (Figure S1 in Supporting Information S1) but the maximum and minimum values occur on average during August and February, respectively, in the NH but vice versa in the SH. Near the equator, the spatial pattern of SST seasonality is more complicated. Figure 2b shows the amplitude of the SST seasonal cycle averaged globally starting from 1851 to 2100 obtained from the historical, RCP 4.5 and RCP 8.5 simulations in CMIP5. It is evident that the amplitude of SST seasonal cycle intensifies over the 21st century in both intermediate (RCP 4.5) and high (RCP 8.5) emission scenarios. The multi-model mean (inter-model spread) of the amplitude of SST seasonal cycle increases by 13% (±8%) and 30% (±20%) toward the end of 21st century under RCP 4.5 and RCP 8.5 scenario, respectively. The inter-model spread is estimated by standard deviation against the multi-model mean. Figure S2b in Supporting Information S1 shows that the intensification is also present in the CMIP6 SSP2-4.5 and SSP5-8.5 scenario simulations.

Alexander et al. (2018) suggested that a reduction in the seasonal cycle of MLD in future (e.g., δh) could contribute to the amplification of the SST seasonal cycle. Figure 2d indicates that the amplitude of MLD seasonal cycle is projected to decrease by 10% and 20% for the RCP 4.5 and RCP 8.5 scenario, respectively. The CMIP6 models project similar decreases in the MLD seasonality (Figure S2c in Supporting Information S1). The weakening is attributable to the larger decrease of MLD during local winter.

The amplification of SST seasonal cycle is spatially non-uniform. Figure 3 shows the change in the amplitude of SST seasonal cycle during the 21 years of 2080–2100 relative to the 21 years of 1985–2005 based on multi-model mean of 13 CMIP5 models under the RCP 8.5 and RCP 4.5 scenario. It is noted that the intensification of the SST seasonal cycle is much larger in the NH than the SH and in the mid- and high latitude rather than tropics. In fact, the pattern of change resembles the mean SST seasonal amplitude (Figure 1) quite closely. The North Atlantic exhibits a higher increase in SST seasonality than the North Pacific, which can be linked to the difference in long-term mean mixed layer shoaling (Figures 3c and 3f), as will be discussed below. We also find a consistent increase in SST seasonality in the equatorial central and eastern Pacific, in agreement with Timmermann et al. (2004), as well as in the equatorial eastern Indian Ocean. The spatial distribution of the projected amplification of the SST seasonality during the end of 21st century is consistent with that in CMIP6 models (Figure S5 in Supporting Information S1) as also shown in Kwiatkowski et al. (2020).

The SST seasonal cycle is projected to intensify mainly as a result of larger warming occurring during local summer as compared to winter (Figure 3). The largest warming occurs during August and September in the North Atlantic (30°–60°N, 50°–10°W) and North Pacific (30°–60°N, 150°E–130°W) and during February and March in the South Indian Ocean (45°–30°S, 60°–120°E).

3.2. Contributing Factors for Amplification of SST Seasonality

Here we examine the main factors responsible for the change in SST seasonal amplitude by computing the simplified non-advective heat budget (see Section 2.2) and using the regional SST maximum and minimum pattern in Figure S1 in Supporting Information S1. Since we neglect the contribution from changes in ocean advection and other vertical processes, the potential driving factors are changes in annual mean (ΔQ) and amplitude of seasonal cycle (δQ_a) of surface net heat flux and annual mean (Δh) and amplitude of seasonal cycle (δh_a) of MLD, as shown in Equation 8. To check if our simplification works, we calculate both $d\delta SST_a/dt$ directly from SST data, and $d\delta T_a/dt$ as the reconstructed change in amplitude of SST seasonal cycle based on the simplified mixed layer temperature equation. Figure S6 in Supporting Information S1 illustrates that the reconstruction can explain a large fraction of the projected change in SST seasonality over most of ocean basins.

ΔQ (change in annual mean heat flux) can contribute to the change in SST seasonal amplitude change. Its contribution is weighted by the ratio of the present-day amplitude of MLD seasonal cycle and the inverse of the square of the present-day annual mean MLD as shown in term 1 of Equation 8 (e.g., $-\frac{\left(h_1'\Delta Q\right)_a}{\rho C_p \overline{h_1}^2}$). Since the MLD is shallower during local summer than local winter, $h_1' < 0$ in general. Thus, the projected increase in ΔQ (Figure 3b) leads to the amplification of SST seasonal cycle particularly in the region where the seasonal MLD difference in the present (h_{1a}') is large (Figure S7 in Supporting Information S1). Figure 4a indicates that the ΔQ factor (term 1, contribution from change in annual mean surface heat flux) induces only a moderate increase in SST seasonality in most of ocean basins and significantly in the North Atlantic.

A positive δQ_a (increase in the amplitude of surface heat flux) can increase the amplitude of the SST seasonal cycle accounting for the inverse proportionality in the annual mean of MLD in the present (Term 2, $\frac{\delta Q_a}{\rho C_p \overline{h_1}}$). However, the increase is compensated in proportion to the ratio between the amplitude of MLD seasonal cycle to the annual mean MLD in the present (Term 3, $\frac{\left(h_1'\delta Q\right)_a}{\rho C_p \overline{h_1}^2}$). In general, the contribution from term 2 is larger than term 3 since $\frac{1}{\overline{h_1}} > \frac{h_{1a}'}{\overline{h_1}^2}$. The net contribution from Terms 2–3 is to decrease SST seasonality over some parts of the North Atlantic and Southern Ocean but to increase over some parts of the North Pacific, South Pacific, South Atlantic, Arctic Ocean and Southern Ocean (Figure 4b).

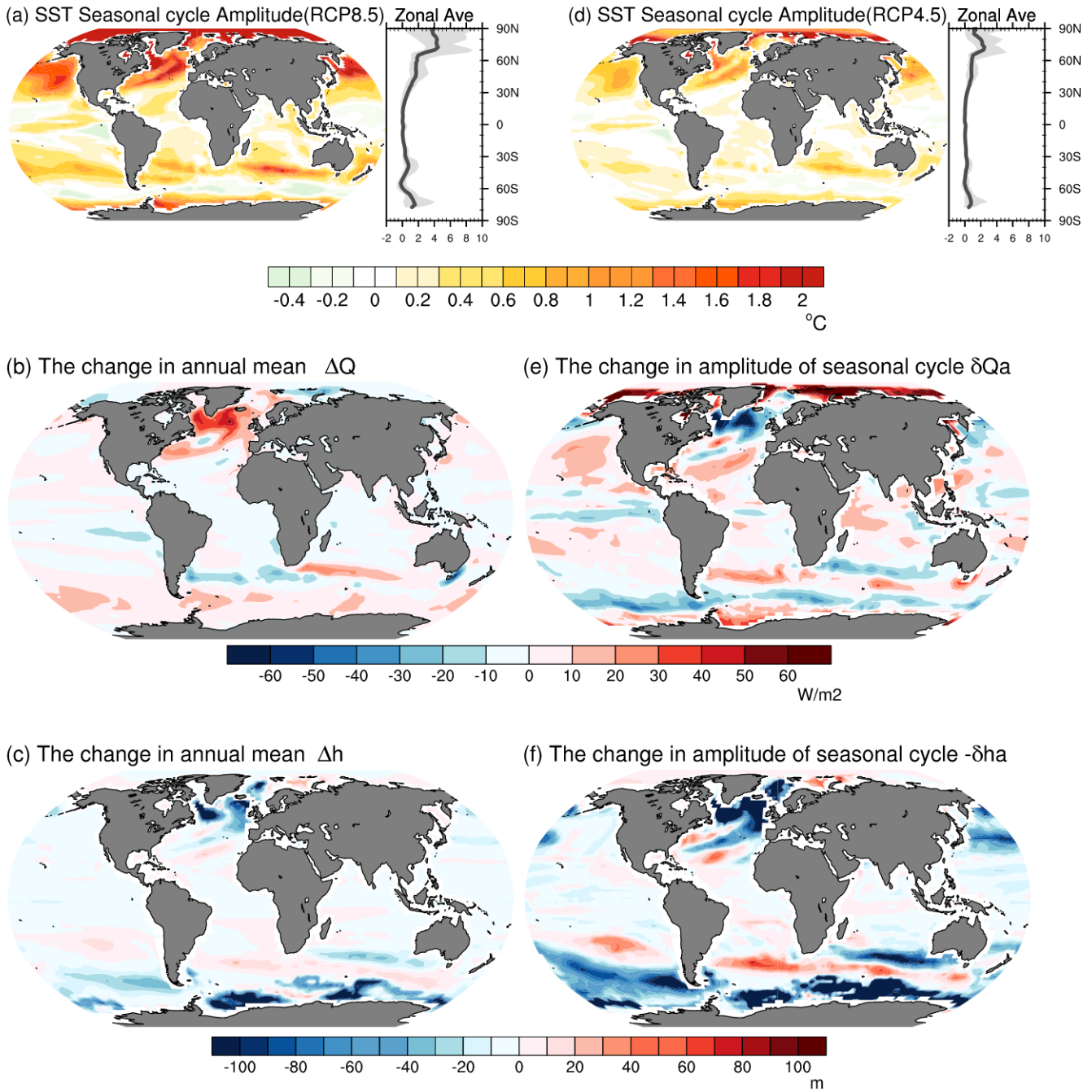

Figure 3. Projected future change in the amplitude of sea surface temperature seasonal cycle during the end of 21st century (2080–2100) relative to the recent past (1985–2005) obtained from 13 models' mean of CMIP5 models under the (a) Representative Concentration Pathway (RCP) 8.5 and (d) RCP 4.5 scenario. Multi-model mean (thick solid line) and inter-model spread (gray shading) of zonal mean of the amplitude are also shown in the right-hand side of map. (b and e) shows the change in annual mean (left) and amplitude (seasonal maximum minus minimum) of seasonal cycle (right) for surface net heat flux and (c and f) for mixed layer depth, respectively, during the end of 21st century (2080–2100) relative to the recent past (1985–2005) period obtained by multi-model mean of 13 CMIP5 models under the RCP8.5 scenario.

Terms 4–6 represent the contributions from Δh (change in annual mean MLD). Since $\frac{1}{\overline{h_1}^2} > \frac{h'_{1a}}{\overline{h_1}^3}$ (mean MLD is larger than MLD seasonal cycle) in general, term 4 is larger than terms 5 and 6. Thus, a decrease in annual mean of MLD (negative Δh) can result in the intensification of SST seasonal cycle weighted by the amplitude of seasonal cycle of surface net heat flux in the present, particularly in the region where the annual mean of MLD

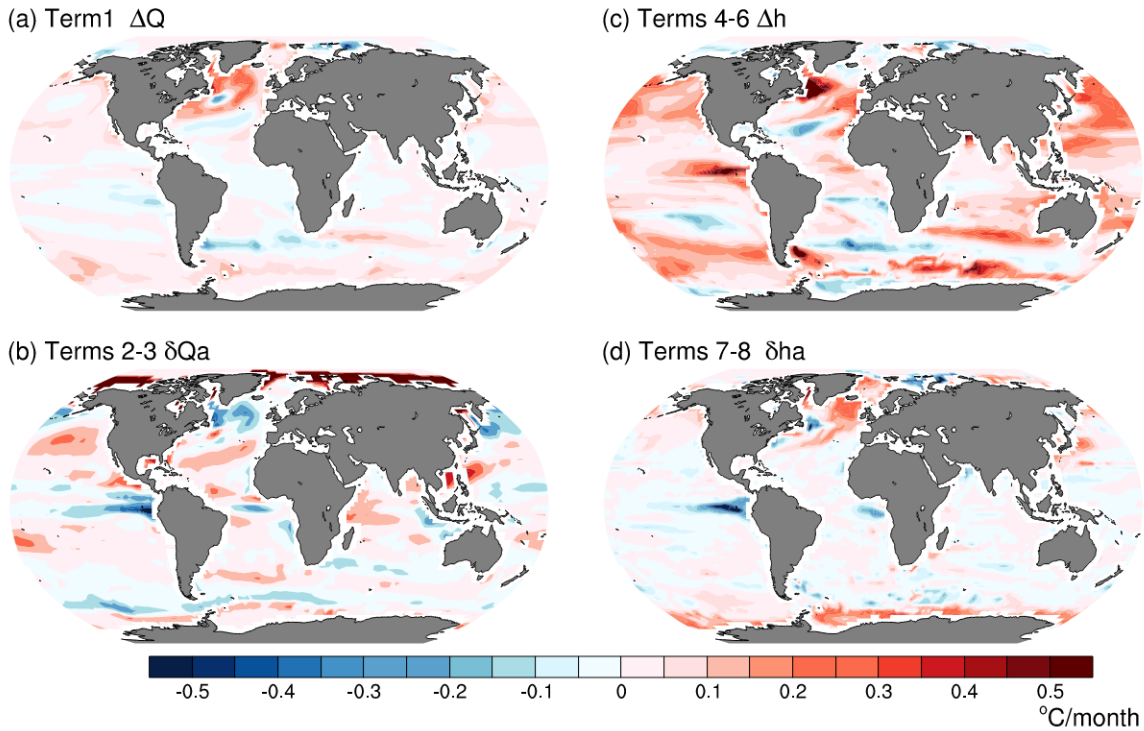

Figure 4. Contributions to the change in the amplitude of sea surface temperature seasonality from panel (a) the ΔQ factor (term1), (b) the δQ_a factor (terms2-3), (c) the Δh factor (terms 4-6), and (d) the δh_a factor (terms 7-8) in Equation 8.

is shallower (term 4, $-\frac{\left(Q_1'\Delta h\right)_a}{\rho C_p \overline{h_1}^2}$). Figure 3c shows that Δh will decrease in most parts of the global ocean which is attributable to the well-documented increase in stratification in response to greenhouse warming. It is noted that the decrease in annual mean of MLD (terms 4–6) plays the dominant role in intensifying SST seasonality in most of ocean basin (Figure 4c).

Figure 3f indicates that δh_a (change in seasonal amplitude of MLD) is projected to decrease in response to global warming, particularly in the region where the robust decrease in the annual mean MLD (Δh) is projected. The contribution from δh_a is determined by the difference between annual mean and amplitude of seasonal cycle of surface net heat flux in the present (e.g., $\left(\overline{Q_1}\delta h\right)_a - \left(Q_1'\delta h\right)_a$) as shown in terms 7 and 8 in Equation 8. In the region where $\overline{Q_1} - Q_1' > 0$, the δh_a will lead to the amplification of SST seasonal cycle. We notice that its contribution is smaller than that of annual-mean MLD change in most of the ocean basins (Figure 4d).

We quantify the contribution from each driver to the amplification of SST seasonal cycle focusing here on the North Atlantic, North Pacific and Southern Indian Ocean where the amplification is particularly strong as shown in Figure 3 and Figure S5 in Supporting Information S1. Figure S8 in Supporting Information S1 shows that the simplified non-advective heat budget for the annual cycle changes explains a considerable fraction of the total diagnosed change from the CMIP5 models with a residual term contributing between 10% and 40% depending on the region. We further see that the decrease in annual mean of MLD attributable to the projected increase in stratification is the most important process leading to the amplification of SST seasonality in all three ocean basins (terms 4–6) (Figure S8 in Supporting Information S1). In particular, term 4 ($-\frac{\left(Q_1'\Delta h\right)_a}{\rho C_p \overline{h_1}^2}$) is comparable to the reconstructed change ($d\delta T_d/dt$) in all three ocean basins.

In the North Atlantic, the increase in annual mean of surface net heat flux (ΔQ) also positively contributes to the increase of the amplitude of the SST seasonal cycle (Figure 4a) while the decrease in seasonal cycle amplitude of surface net heat flux (Figure 4b) over the North Atlantic tends to slightly reduce the amplitude of SST seasonal

cycle. The residual term explains about 40% of the projected increase in amplitude of SST seasonal cycle. To summarize, the majority of the amplification of SST seasonality over the North Atlantic can be explained in terms of the annual mean change of MLD and surface net heat fluxes.

In the North Pacific, the annual mean change of MLD (Δh) plays a dominant role to increase the amplitude of SST seasonal cycle. There are slight positive contributions from the annual mean change of surface net heat flux (ΔQ) and seasonal cycle change of MLD (δh_a). In the South Indian Ocean, the terms that contribute to the seasonal cycle amplitude of SST is similar with North pacific with less magnitude. Increase in annual mean change of surface net heat flux (ΔQ) and annual mean change of MLD (Δh) contribute to increase the amplitude of SST seasonal cycle in the South Indian Ocean basin. The residual term (Figure S9 in Supporting Information S1) explains about 15% and 30% of the projected increase in amplitude of SST seasonal cycle in the North Pacific and South Indian Ocean, respectively.

4. Discussions and Conclusions

Using the output from 13 coupled models in CMIP5, our study provides a comprehensive analysis of the characteristics and driving mechanisms responsible for the intensification of the seasonal cycle of SST. Globally, by the end of 21st century the amplitude of the SST seasonal cycle increases by 13% (±8%) and 30% (±20%) for RCP4.5 and RCP8.5 scenarios, respectively and the projected ocean warming over summertime is much stronger than winter. We demonstrate that on average the global amplification of seasonal cycle of SST can be explained in terms of the increase in stratification that will trap the seasonal heat flux variability to a shallower layer. The intensification of the SST seasonal cycle is much larger over NH than the Southern Hemisphere and in the mid and high latitudes than tropics. The amplification rate for individual ocean basins is different and we observe the largest amplification in areas with a deep climatological mixed layer. Therefore, our study focuses on three Ocean basins where the amplification is robust (based on seasonal cycle, Figures 3a, 3d, and S5 in Supporting Information S1), that is, North Atlantic Ocean, North Pacific Ocean, and South Indian Ocean.

To better understand the main mechanisms controlling the amplification of SST seasonality, we conducted a simplified heat budget analysis for the surface heat flux component of mixed layer temperature equation. In three ocean basins as mentioned above, it is found that the decrease in annual mean MLD due to the increase in stratification is the most important contributor of the amplification of SST seasonal cycle. Increases in annual mean of net surface heat flux play a secondary role just in the North Atlantic with slight compensation from the decrease in seasonal cycle amplitude of net surface heat flux.

The intensification in the seasonal cycle of SST might have implications for future changes in the ecosystems. A seasonal cycle amplification may add to the existing stressors to ecosystems such as ocean acidification and reduced upper ocean oxygen levels. Therefore, understanding the drivers of SST seasonal cycle intensification in response to greenhouse warming may help to better determine the productivity and distribution of marine species in future.

Our heat budget analysis has a number of limitations as we ignored the advection and other vertical processes of the heat budget. It is estimated that the advection term explains about 10%–40% of the change in SST seasonality depending on the region. Future research will focus on the effects of ocean circulation changes on seasonal SST variability and its response to greenhouse warming. Other sources of limitations are our assumption on $h' \ll \overline{h}$ and $\Delta h \ll \overline{h}_1$ which may not hold in polar regions and Labrador Sea and neglection of potential shifts in SST seasonal cycle in a warmer world.

It is important to note that integrated observed data indicate the deepening of summertime MLD as well as the increase of the upper ocean stratification on a global scale from 1970 to 2018 (Sallée et al., 2021) which may be contradictory to recent modeling studies and the current study suggesting increases in upper ocean stratification and shoaling of MLD in response to global warming. Large uncertainties remain in both observations mainly due to sparse coverage and models due to imperfect parameterization. This calls for further investigation to better estimate observed changes and their drivers as well as further improvement in ocean models with higher horizontal and vertical resolution and better representation of vertical mixing processes (Donald & Kathleen, 2014).

Conflict of Interest

The authors declare no conflicts of interest relevant to this study.

Data Availability Statement

The CMIP5 and CMIP6 data are all available at https://esgf-node.llnl.gov/search/cmip5/ *and at* https://esgf-node.llnl.gov/search/cmip6/. *The NOAA_ERSST_V4 data provided by the NOAA/OAR/ESRL PSL, Boulder, Colorado, USA, publicly available at* https://www.esrl.noaa.gov/psd/data/gridded/data.noaa.ersst.html.

Acknowledgments
A. R. Jo, J.-Y. Lee, A. Timmermann, and R, Yamaguchi were supported by the Institute for Basic Science (project code IBS-R028-D1). J-Y. Lee was also supported by the National Research Foundation (NRF-2019R1I1A3A01058290) in Korea. Authors thank Dr. Jung-Eun Chu for supporting with coding and Mr. Arjun Babu Nellikkattil for helping to download CMIP5 and CMIP6 model data. We thank the World Climate Research Programme's Working Group on Coupled Modelling, which is responsible for CMIP, the climate modeling groups for producing and making available their model output (listed in Section 2.1), the Earth System Grid Federation (ESGF) for archiving the data and providing access, and the multiple funding agencies who support CMIP5 and CMIP6 and ESGF.

References

Alexander, M. A., Scott, J. D., Friedland, K. D., Mills, K. E., Nye, J. A., Pershing, A. J., & Thomas, A. C. (2018). *Projected sea surface temperatures over the 21st century: Changes in the mean, variability and extremes for large marine ecosystem regions of northern oceans*. Elementa 6. https://doi.org/10.1525/elementa.191

Bjerknes, J. (1969). Atmospheric teleconnections from the equatorial Pacific 1. *Monthly Weather Review*, *97*(3), 163–172. https://doi.org/10.1175/1520-0493(1969)097<0163:atftep>2.3.co;2

Chen, C., & Wang, G. (2015). Role of North Pacific mixed layer in the response of SST annual cycle to global warming. *Journal of Climate*, *28*(23), 9451–9458. https://doi.org/10.1175/JCLI-D-14-00349.1

Chen, Y. Y., & Jin, F. F. (2018). Dynamical diagnostics of the SST annual cycle in the eastern equatorial Pacific: Part I a linear coupled framework. *Climate Dynamics*, *50*(5–6), 1841–1862. https://doi.org/10.1007/s00382-017-3725-7

Deser, C., Alexander, M. A., Xie, S.-P., & Phillips, A. S. (2010). Sea surface temperature variability: Patterns and mechanisms. *Annual Review of Marine Science*, *2*(1), 115–143. https://doi.org/10.1146/annurev-marine-120408-151453

Donald, K. P., & Kathleen, F. J. (2014). Journal of geophysical research oceans. *Journal of Geophysical Research: Oceans*, *119*, 3868–3882. https://doi.org/10.1002/2013JC009535

Eyring, V., Bony, S., Meehl, G. A., Senior, C. A., Stevens, B., Stouffer, R. J., & Taylor, K. E. (2016). Overview of the Coupled Model Intercomparison Project Phase 6 (CMIP6) experimental design and organization. *Geoscientific Model Development*, *9*(5), 1937–1958. https://doi.org/10.5194/gmd-9-1937-2016

Federation, K. R., & Lynne, D. (2013). Observations: Ocean. In *Climate change 2013: The physical science basis* (Vol. 255–316). https://doi.org/10.1017/CBO9781107415324.010

Gallego, A. M., Timmermann, A., Friedrich, T., & Zeebe, R. E. (2018). Drivers of future seasonal cycle changes in oceanic pCO_2. *Biogeosciences*, *15*(17), 5315–5327. https://doi.org/10.5194/bg-15-5315-2018

Gleckler, P. J., Santer, B. D., Domingues, C. M., Pierce, D. W., Barnett, T. P., Church, J. A., et al. (2012). Human-induced global ocean warming on a multidecadal timescales. *Nature Climate Change*, *2*(7), 524–529. https://doi.org/10.1038/nclimate1553

Huang, B., Thorne, P. W., Banzon, V. F., Boyer, T., Chepurin, G., Lawrimore, J. H., et al. (2017). Extended reconstructed sea surface temperature, version 5 (ERSSTv5): Upgrades, validations, and intercomparisons. *Journal of Climate*, *30*(20), 8179–8205. https://doi.org/10.1175/JCLI-D-16-0836.1

IPCC. (2019). The Ocean and cryosphere in a changing climate. A special report of the intergovernmental panel on climate change. *Intergovernmental Panel on Climate Change*, 1–765.

Karamperidou, C., Stuecker, M. F., Timmermann, A., Yun, K. S., Lee, S. S., Jin, F. F., et al. (2020). Challenges, paleo-perspectives, and outlook. In *ENSO in a changing climate* (pp. 471–484). https://doi.org/10.1002/9781119548164.ch21

Kwiatkowski, L., Torres, O., Bopp, L., Aumont, O., Chamberlain, M., Christian, J., et al. (2020). Twenty-first century ocean warming, acidification, deoxygenation, and upper ocean nutrient decline from CMIP6 model projections. *Biogeosciences Discussions*, *17*(13), 3439–3470. https://doi.org/10.5194/bg-2020-16

Liu, F., Lu, J., Luo, Y., Huang, Y., & Song, F. (2020). On the oceanic origin for the enhanced seasonal cycle of SST in the midlatitudes under global warming. *Journal of Climate*, *33*(19), 8401–8413. https://doi.org/10.1175/JCLI-D-20-0114.1

Sallée, J. B., Pellichero, V., Akhoudas, C., Pauthenet, E., Vignes, L., Schmidtko, S., et al. (2021). Summertime increases in upper-ocean stratification and mixed-layer depth. *Nature*, *591*(7851), 592–598. https://doi.org/10.1038/s41586-021-03303-x

Schmitt, R. (2018). The Ocean's role in climate. *Oceanography*, *31*(2). https://doi.org/10.5670/oceanog.2018.225

Schulzweida. (2017). CDO user guide. *Climate Data Operators. Version 1.9.1*. Retrieved from https://code.mpimet.mgp.de/projects.cdo/embedded/cdo.pdf

Sunagawa, S., Coelho, L. P., Chaffron, S., Kultima, J. R., Labadie, K., Salazar, G., et al. (2015). Structure and function of the global ocean microbiome. *Science*, *348*(6237), 1261359. https://doi.org/10.1126/science.1261359

Taylor, K. E., Stouffer, R. J., & Meehl, G. A. (2012). An overview of CMIP5 and the experiment design. *Bulletin of the American Meteorological Society*, *93*(4), 485–498. https://doi.org/10.1175/BAMS-D-11-00094.1

Thomas, M. K., Kremer, C. T., Klausmeier, C. A., & Litchman, E. (2012). A global pattern of thermal adaptation in marine phytoplankton. *Science*, *338*(6110), 1085–1088. https://doi.org/10.1126/science.1224836

Timmermann, A., Jin, F.-F., & Collins, M. (2004). Intensification of the annual cycle in the tropical Pacific due to greenhouse warming. *Geophysical Research Letters*, *31*(12), L12208. https://doi.org/10.1029/2004GL019442

Yamaguchi, R., & Suga, T. (2019). Trend and variability in global upper-ocean stratification since the 1960s. *Journal of Geophysical Research: Oceans*, *124*(12), 8933–8948. https://doi.org/10.1029/2019JC015439